JOC The Journal of Organic Chemistry

Article

pubs.acs.org/joc

# Pyrene−Oxadiazoles for Organic Light-Emitting Diodes: Triplet to Singlet Energy Transfer and Role of Hole-Injection/Hole-Blocking Materials

Swetha Chidirala,[†] Hidayath Ulla,[§] Anusha Valaboju,[‡] M. Raveendra Kiran,[§] Maneesha Esther Mohanty,[†] M. N. Satyanarayan,*[,§] G. Umesh,[§] Kotamarthi Bhanuprakash,*[,‡] and Vaidya Jayathirtha Rao*[,†,∥]

[†]Crop Protection Chemicals Division and AcSIR, CSIR-Indian Institute of Chemical Technology, Uppal Road Tarnaka, Hyderabad 500007, India

[‡]Inorganic and Physical Chemistry Division, Indian Institute of Chemical Technology, Uppal Road Tarnaka, Hyderabad 500007, India

[§]Optoelectronics Laboratory, Department of Physics, National Institute of Technology Karnataka, Surathkal, Mangalore 575025, India

[∥]Network Institute for Solar Energy, New Delhi 110012, India

Supporting Information

**ABSTRACT:** Three pyrene−oxadiazole derivatives were synthesized and characterized by optical, electrochemical, thermal, and theoretical investigations to obtain efficient multifunctional organic light emitting diode (OLED) materials. Synthesized molecules were used as emitters and electron transporters in three different device configurations, involving hole-injection/hole-blocking materials that showed good current and power efficiencies. To understand the underlying mechanisms involved in the application of these molecules as emitters and transporters, a detailed photophysical characterization of molecules **4**−**6** was carried out. The absorption, steady-state fluorescence, phosphorescence, fluorescence lifetime, and phosphorescence lifetime measurements were carried out. The high quantum yield and efficient reverse intersystem crossing leading to delayed fluorescence emission makes the molecule a good emitter, and the charge delocalization properties leading to excimer formation make them efficient electron transporters. Isoenergetic singlet and triplet states of the molecules make the reverse intersystem crossing feasible at room temperature even in the absence of thermal activation.

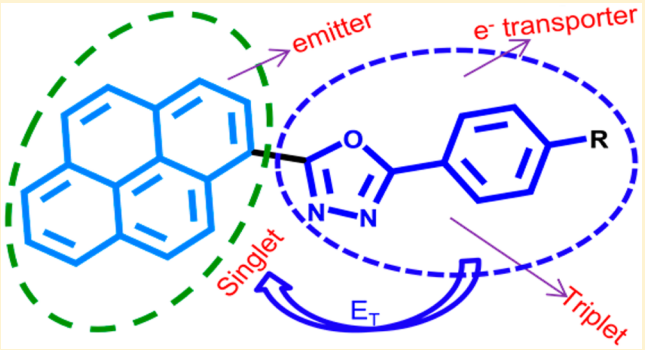


## INTRODUCTION

The work by Tang and VanSlyke in 1987[1] introduced organic light emitting diodes (OLEDs) having applications in flat panel displays and solid-state lighting resources. Subsequently, a huge academic interest has developed in the field of OLEDs.[2,3] OLEDs have several advantages like low driving voltage, high brightness, full-color emission, fast response time, wide viewing angle, and self-emitting properties with low cost and improved performances.[4] The search for stable and highly efficient primary color (red, green, and blue) emitters is extremely important for the commercial application of OLEDs.[5−7] Developing new emitting materials and optimizing the device architectures can lead to improved efficiency and lifetime of OLEDs.[8] Spin statistics indicate that the fluorescent OLEDs can have a maximum of 25% quantum efficiency ($\eta_{int}$), whereas phosphorescent OLEDs (PhOLEDs) can achieve a $\eta_{int}$ value of 100%.[9] Although phosphorescent OLEDs have reached their $\eta_{int}$ limit,[10] they have some disadvantages, including lower electroluminescence (ECL) efficiency under high current densities[11] and rather low reliability in the blue region of the visible spectrum for practical applications. The thermally activated delayed fluorescence (TADF) phenomenon facilitates the harvesting of triplets in to singlets resulting in enhanced fluorescence leading to higher efficiencies.[12−14] The TADF phenomenon attracted researchers to design new molecules with improved properties and higher efficiencies.[15,16]

The electron-deficient moieties like pyridine,[17] oxadiazole,[18−20] triazine,[21] phenathroline,[22] benzimidazole,[23] quinolines,[24] phosphine oxide,[25] and quinoxalines[26] are known to be good electron conductors and with various core structures have been used as electron-transport materials in OLEDs. Oxadiazoles are excellent electron transporting/hole blocking materials used in OLEDs due to their electron deficient

**Received:** October 27, 2015
**Published:** December 10, 2015





DOI: 10.1021/acs.joc.5b02423
J. Org. Chem. 2016, 81, 603−614

**Scheme 1. Synthetic Route of Compounds 4−7**

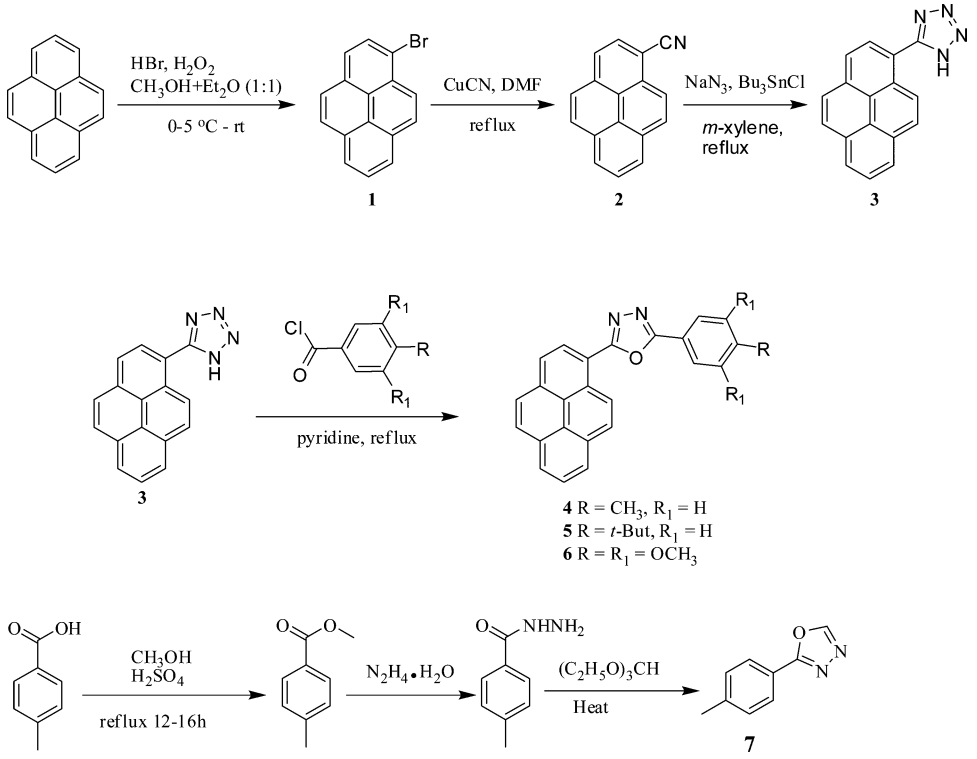


nature.[18−20] Their derivatives have also been reported to have over 20% external quantum efficiency in red, green, and blue PhOLEDs. Incorporation of the oxadiazole group enhances thermal stability, which is an essential property of OLED material.[27]

Pyrene is employed as a building block for organic optoelectronic materials, particularly in OLEDs, due to its strong fluorescence emission and charge transport ability.[28−30] However, the high tendency toward $\pi-\pi$ stacking of the pyrene moieties generally lends the pyrene-containing emitters strong intermolecular interactions in the solid state, which leads to a substantial red shift of their fluorescence emission and a decrease of the fluorescence quantum yields ($\Phi_f$).[31] Various pyrene-based light-emitting materials have been reported in the recent literature, including functionalized pyrene-based light-emitting molecules,[32,33] functionalized pyrene-based light-emitting dendrimers,[34,35] oligomers, and polymers.[36] To date, many kinds of pyrene-based materials have been synthesized and considered for several applications, and some of them proved to be promising blue emitters for OLEDs. Pyrene coupled with carbazole dendrimers were synthesized by Keawin et al. to obtain multifunctional materials that behave as blue emitters and hole-transporting materials.[37] Another pyrene-based multifunctional molecule was synthesized by Mallesham et al., which could be used as a blue emitter and electron-transporting material.[25] A pyrene-appended dimethyl phenyl derivative was used (Chou et al.) to harvest the triplet states through reverse intersystem crossing.[38] Previously, there have been reports on pyrene compounds, but most of them are blue-emitting materials.[39,40] Pyrene-functionalized triphenylamine-based dyes as green-emitting materials in OLEDs have been reported by Lu et al.[41] However, pyrene-functionalized green emitters for OLEDS were less explored.

With an aim toward developing efficient electron-transporting green emitters, we investigated three new oxadiazole-appended pyrene derivatives wherein pyrene acts as an emitter and oxadiazole as an electron transporter. These compounds exhibited excellent thermal stability, high fluorescence quantum yields, and appropriate HOMO/LUMO energy levels making them promising multifunctional green emitters. Device data indicated that these compounds showed excellent device characteristics which can be attributed to reverse intersystem crossing involving oxadiazole and pyrene units of the molecule and further excimer formation leading to luminescence. Use of suitable hole injection agent or hole-blocking material played an important role in obtaining higher efficiencies. The observed delayed fluorescence emission along with complete overlap of oxadiazole phosphorescence with pyrene fluorescence is cited as supporting evidence for the proposed mechanism.

## RESULTS AND DISCUSSION

**Synthesis and Characterization.** Scheme 1 illustrates the design and synthesis of three pyrene−oxadiazole derivatives (Figure 1), namely, **4** (2-(pyren-1-yl)-5-*p*-tolyl-1,3,4-oxadiazole), **5** (2-(4-*tert*-butylphenyl)-5-(pyren-1-yl)-1,3,4-oxadiazole), **6** (2-(pyren-1-yl)-5-(3,4,5-trimethoxyphenyl)-1,3,4-oxadiazole), and **7** (2-*p*-tolyl-1,3,4-oxadiazole). The synthetic procedure adopted to obtain the target materials **4**−**7** (Figure 1) is given in Scheme 1. Pyrene was brominated[42] to obtain bromopyrene **1**. Conversion of the bromo derivative to nitrile **2** was achieved by Rosenmund−von Braun synthesis[43] using cuprous cyanide. Freshly prepared $Bu_3SnN_3$ was used to obtain tetrazole intermediate **3**.[44] In the final step, compound **3** was treated with the different acid chlorides to obtain target compounds **4**−**6**. 4-Methylbenzoic acid was esterified, treated with hydrazine hydrate, and then reacted with trimethyl orthoformate to get the targeted 2-*p*-tolyl-1,3,4-oxadiazole


DOI: 10.1021/acs.joc.5b02423
J. Org. Chem. 2016, 81, 603−614

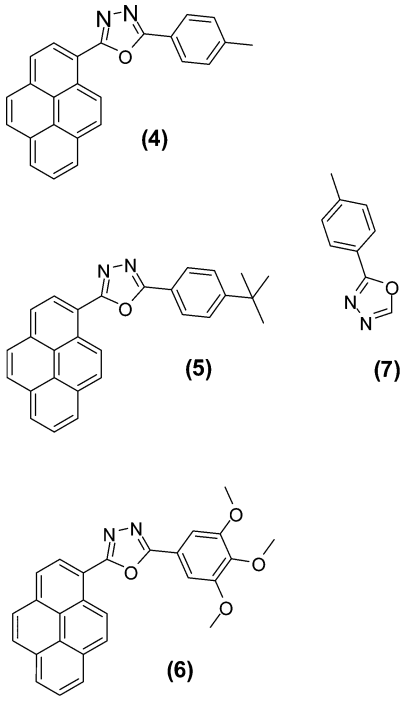


**Figure 1.** Chemical structures of the target compounds **4**–**7**.

(**7**). All the compounds were fully characterized by spectroscopic methods. The details of the experimental characterization data are available in the Supporting Information.

**Photophysical Properties.** UV–vis absorption spectra and photoluminescence of the compounds **4**–**6** were recorded in a series of solvents of different polarities, viz. hexane, toluene, THF, chloroform, acetonitrile, and methanol. The absorption and photoluminescence spectral data of compounds **4**–**6** are presented in Tables 1 and 2. Representative absorption and emission spectra in solution and thin film are shown in Figures 2 and 3. A typical UV–vis spectrum of pyrene has a structured absorption between 250 and 350 nm. In comparison with pyrene, the absorption spectra of compounds **4**–**6** are red-shifted due to attachment of the oxadiazole moiety to pyrene and slightly broadened due to the introduction of charge delocalization in the system. The bands between 360 and 394 nm are ascribed to the $\pi$–$\pi^*$ transition of the pyrene moiety (Figure 2). The absorption spectra in thin films are red-shifted by ∼10 nm relative to those in solution (Figure 2b). Fluorescence emission maxima are observed for these three compounds **4**–**6** are in the range of 420–460 nm (Table 2) in solution, whereas in thin film they are red-shifted to 510–530 nm. On changing the solvent polarity from hexane to acetonitrile, a small 5–10 nm shift was observed in the samples (**4**–**6**). The fluorescence emission spectra of the compounds in chloroform is structured, and on casting films the spectra become broadened (Figure 3). Thin film fluorescence studies indicate that there are intermolecular interactions in the excited state, leading to over 60 nm red shift. The structured shape of fluorescence in solution (Figure 3a) and the broad structureless fluorescence in thin film (Figure 3b) also indicates intermolecular interactions in the excited state. The quantum yields of fluorescence measured for these compounds are over 85% (Table 2). Further fluorescence studies were carried out by varying the concentration in order to monitor any possible excimer formation in the molecule, and it was found that there is no significant difference (SI). Compound **7** (2-*p*-tolyl-1,3,4-oxadiazole) was synthesized, and its photophysical properties were evaluated for the purpose of comparison. UV–vis absorption (Figure 4a), fluorescence (Figure 4b), and phosphorescence (Figure 5) measurements were carried out. Phosphorescence lifetime for **7** was measured, data was fitted monoexponentially, and the lifetime was 464 $\mu$s. Phosphorescence of the oxadiazole derivative (**7**) has an excellent overlap with fluorescence of all the compounds **4**–**6** (Figure 5). The spectral overlap established (Figure 5) indicates that the triplet to singlet intramolecular energy transfer is an energetically feasible process. The fluorescence lifetimes of compounds **4**–**6** at $10^{-5}$ and $10^{-2}$ M concentrations were measured using a time-correlated single-photon counting technique, and the decays are shown in Figure 6. The decays were fitted monoexponentially, and the fluorescence lifetime of molecules **4**–**6** were found to be between 1 and 3 ns (Table 3). The excited-state lifetime of pyrene monomer is known to be between 100 and 450 ns in different solvents.[45,46] A tremendous decrease in the fluorescence lifetime of the synthesized molecules in comparison to pyrene monomer was observed, probably due to addition of the phenyl oxadiazole group. This is in accordance with the previous reports where pyrene lifetime reduced on attaching single[47] or multiple phenyl rings.[48] Phosphorescence measurements were carried out to identify the triplet states. Interestingly, a delayed fluorescence emission band was observed using 0.06 ms (60 $\mu$s) delay after flashing the lamp (SI). Time-resolved delayed fluorescence studies were carried out at emission maxima and the decays fitted monoexponentially (Table 4). Delayed fluorescence (DF) lifetimes are in microsecond time scales, which are important for display applications. It is well established that a long-lived triplet species may reduce the performance of OLED devices.[49] Thermally activated delayed fluorescence (TADF) is recently studied extensively for applications in OLED, and molecules having TADF show an increase in device efficiency. Close-lying triplet and singlet states are a prerequisite for TADF. The intensity of TADF emission increases with temperature. However, for samples **4**–**6** there was no increase in fluorescence intensity on increasing the temperature from 0 to 35 °C, implying that the intramolecular triplet to singlet energy transfer/conversion does not require thermal activation. The other known form of delayed fluorescence is via triplet–triplet annihilation. No emission was observed from the triplet state; hence, it is impossible to estimate the role of triplet–

**Table 1. UV–vis Absorption Data of Compounds 4–6 in Different Solvents ($10^{-5}$ M) and in Thin Film State**

| compd | hexane (nm) | toluene (nm) | THF (nm) | $CHCl_3$ (nm) | $CH_3CN$ (nm) | $CH_3OH$ (nm) | thin film (nm) | $\lambda_{abs(calcd)}$ ($f$)[a] |
|---|---|---|---|---|---|---|---|---|
| **4** | 286, 364, 391 | 289, 370, 394 | 287, 367, 392 | 268, 369, 394 | 284, 364, 390 | 285, 364, 391 | 292, 381, 403 | 390 (0.8545) |
| **5** | 287, 365, 391 | 289, 370, 394 | 279, 367, 392 | 288, 364, 394 | 285, 364, 390 | 285, 365, 391 | 287, 390, 402 | 388 (0.8613) |
| **6** | 280, 368,392 | 286, 373, 396 | 282, 371, 393 | 283, 372, 396 | 281, 367, 391 | 280, 368, 392 | 291, 394, 407 | 390(0.8523) |

[a]Calculated at the PBE0/6-311g(d,p) level of theory in chloroform solvent; $f$ = oscillator strength.



DOI: 10.1021/acs.joc.5b02423
J. Org. Chem. 2016, 81, 603–614

**Table 2. Fluorescence Data of Compounds 4–6 in Different Solvents and in Thin Film State**[a]

| compd | hexane (nm) | toluene (nm) | THF (nm) | $CHCl_3$ (nm) | $CH_3CN$ (nm) | $CH_3OH$ (nm) | thin film[b](nm) | $\Phi_f$[c] | $\lambda_{em}$[d] |
|---|---|---|---|---|---|---|---|---|---|
| **4** | 418, 447 | 425, 451 | 425, 449 | 426, 450 | 423, 449 | 426, 452 | 511 | 0.85 | 444 |
| **5** | 418, 443 | 426, 453 | 423, 450 | 426, 456 | 423, 452 | 425, 458 | 517 | 0.85 | 445 |
| **6** | 423, 450 | 428, 459 | 426, 458 | 428, 457 | 427, 456 | 430, 457 | 531 | 0.90 | 478 |

[a]All compounds were measured with $10^{-5}$ M concentration at rt; excitation at 390 nm. [b]Measured in the solid state at rt. [c]Fluorescence yields relative to 9,10-diphenyl anthracene ($\Phi$ = 0.95 in cyclohexane). [d]Calculated at SS-PCM//PBE0/6-31+g(d,p) level of theory in chloroform solvent. Emissions at LR-PCM//PBE0/6-31+g(d,p) level of theory in chloroform solvent are 480, 480, and 486 nm for **4**, **5**, and **6**, respectively.

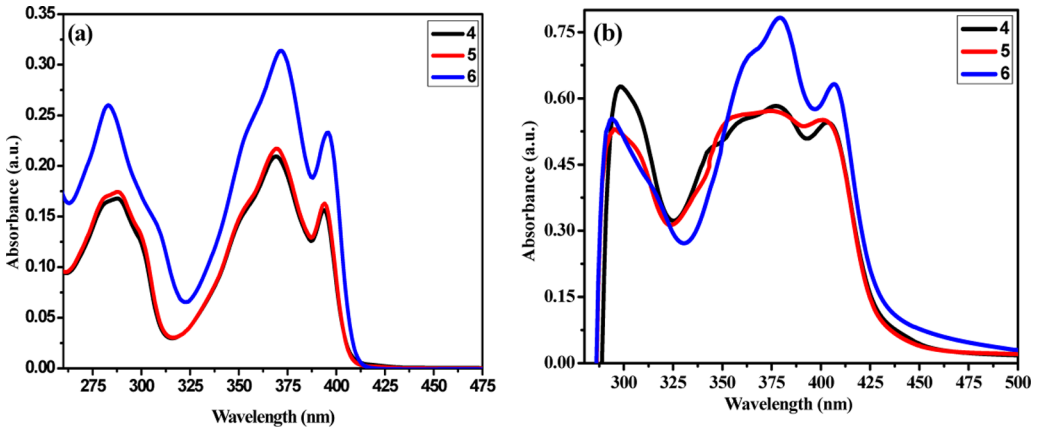


**Figure 2.** UV–vis absorption spectra of compounds **4–6** in (a) $CHCl_3$ at $10^{-5}$ M concentration; (b) thin film state.

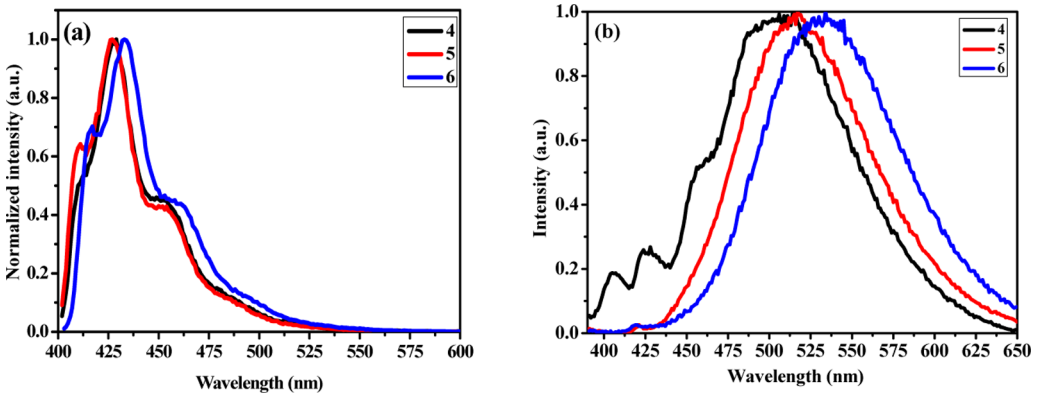


**Figure 3.** Photoluminescence spectra of compounds **4–6** in (a) $CHCl_3$ at $10^{-5}$ M concentration; (b) thin film state. $\lambda_{ex}$ = 370 nm.

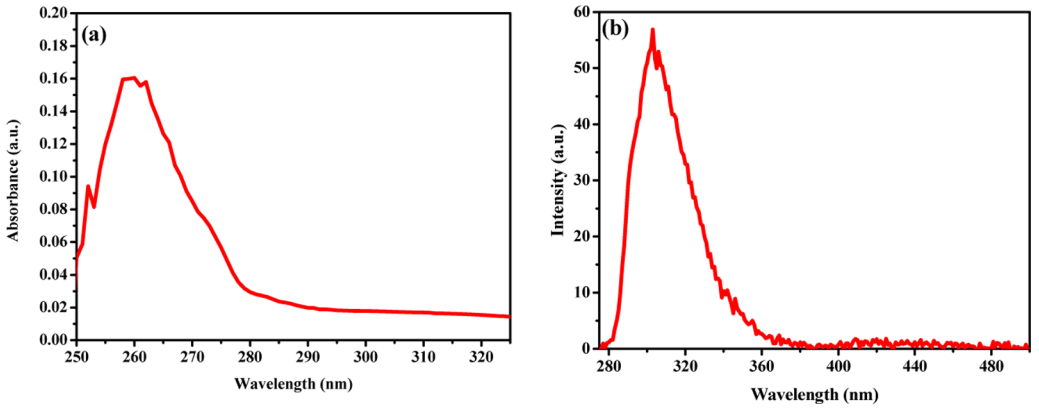


**Figure 4.** (a) UV–vis absorption (b) fluorescence of 2-*p*-tolyl-1,3,4-oxadiazole (**7**) at $10^{-5}$ M concentration. $\lambda_{ex}$ = 260 nm.

triplet annihilation as it is characterized by comparing the triplet and singlet lifetimes.[50] A similar observation was made by Chou. et al. in pyrene-based molecules that showed delayed fluorescence, and it could not be assigned as TADF. Due to high fluorescence quantum yield, the phosphorescence peak could not be experimentally observed.[38] However, due to



DOI: 10.1021/acs.joc.5b02423
J. Org. Chem. 2016, 81, 603–614

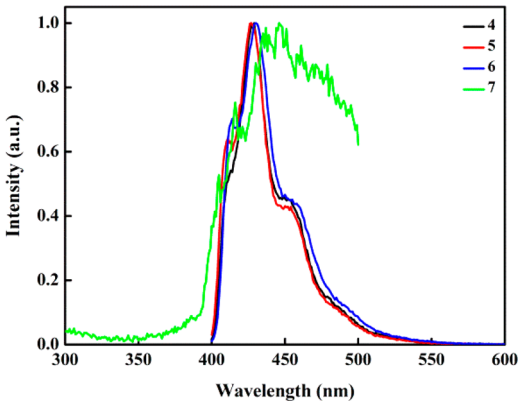


**Figure 5.** Fluorescence spectra of compounds **4**–**6** ($\lambda_{ex}$ = 370 nm) and phosphorescence spectra of 2-*p*-tolyl-1,3,4-oxadiazole (**7**) in green ($\lambda_{ex}$ = 260 nm).

delocalization of charges within the molecule as observed by the structureless fluorescence emission and our previous report on pyrene-based blue emitters, a CT state might improve the possibility of reverse intersystem crossing.[25] Another possibility was explained by measuring the triplet emission of pyrene and oxadiazole separately. The pyrene phosphorescence emission maxima was observed at 590 nm as reported previously,[51] and the oxadiazole triplet peak is observed at 440 nm (Figure 5) with no significant spectral overlap. However, the spectral overlap between the oxadiazole triplet state and the singlet states of pyrene derivatives (**4**-**6**) may support the triplet to singlet energy transfer (Figure 5).

**Theoretical Calculations.** To gain further insight into the electronic structures and their excited states, DFT and TDDFT calculations were performed. The DFT-calculated optimized geometries of molecules **4**–**6** (Figure 7) in the gas phase show slightly twisted conformations. Oxadiazole has a ∼25° tilt with respect to the pyrene plane in all of the molecules, whereas the excited-state optimized geometries at both $S_1$ and $T_1$ are very planar and rigid (Figure 7). The HOMO and LUMO of the molecules are mostly on the pyrene part, and HOMO−1 and LUMO+1 are mostly upon the nonpyrene part.

The singlet excitation energies were obtained from TDDFT calculations and are included in Table 1 for comparison with experimental data. The most intense peak in **4** is at 390 nm with oscillator strength $f$ = 0.8545. In molecule **5**, it is at 388 nm with $f$ = 0.8613. In molecule **6**, it is at 390 nm, with $f$ = 0.8523. It is clear that a small charge transfer occurs from the pyrene part to the nonpyrene part. The substituent showed less impact on the absorption phenomenon in these molecules. The calculated emission energies using TDDFT are included in Table 2. The emission energies are 444 nm for **4**, 445 nm for **5**,

**Table 3. Fluorescence Lifetimes of Compounds 4–6 in Nanoseconds**

| compd | $10^{-5}$ M | $10^{-2}$ M |
|---|---|---|
| **4** | 1.87 | 3.01 |
| **5** | 1.88 | 2.77 |
| **6** | 1.73 | 2.60 |

**Table 4. Delayed Fluorescence Lifetimes of Compounds 4–6 at rt in Microseconds**

| compd | $10^{-5}$ M | $10^{-2}$ M 420 nm | $10^{-2}$ M 525 nm |
|---|---|---|---|
| **4** | 14 | 19 | 16 |
| **5** | 16.8 | 17 | 9.5 |
| **6** | 15 | 17.4 | 16.7 |

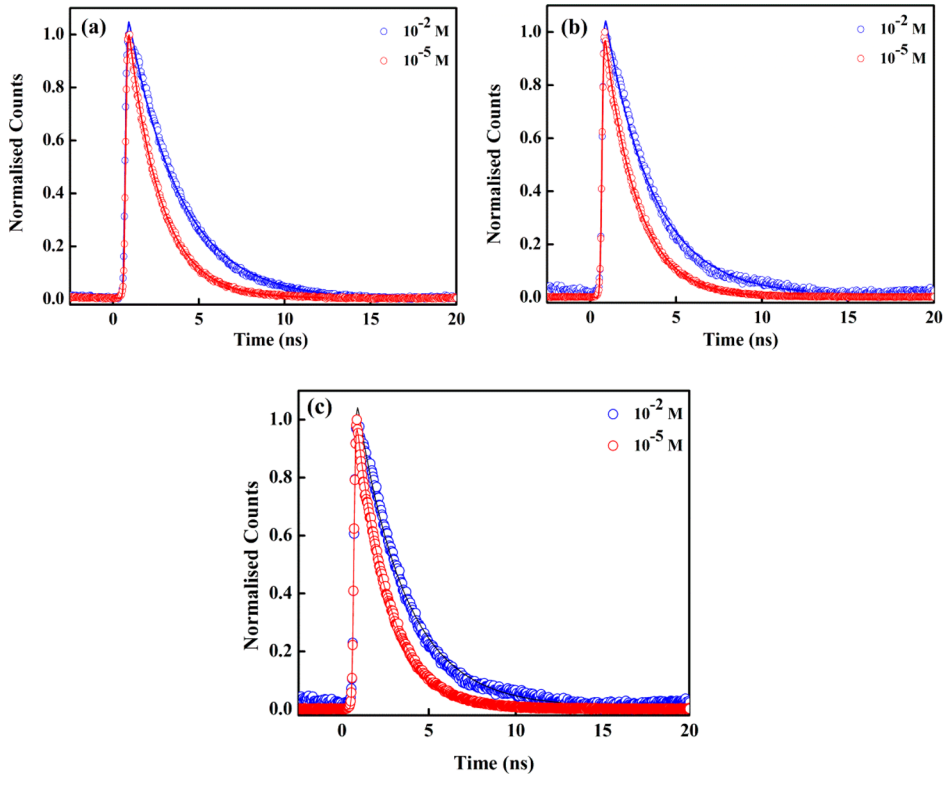


**Figure 6.** Fluorescence lifetime decay curves of compounds (a) **4**, (b) **5**, (c) **6**.



DOI: 10.1021/acs.joc.5b02423
*J. Org. Chem.* 2016, 81, 603–614

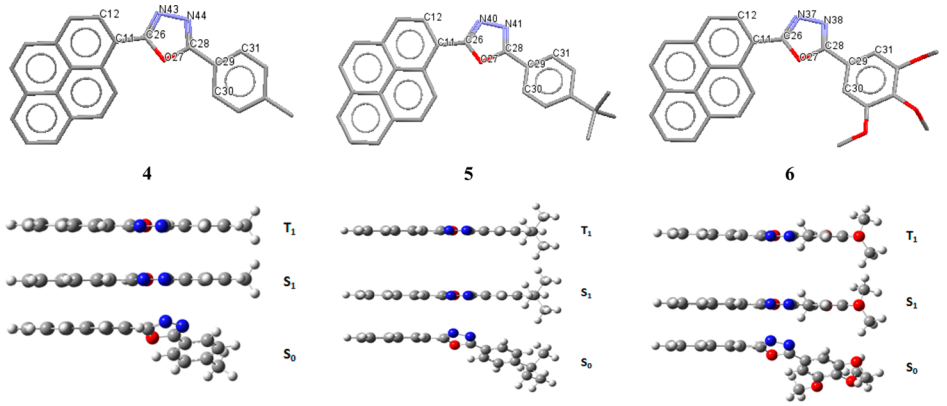


| 4 | 5 | 6 |
|---|---|---|
| $C_{12}$-$C_{11}$-$C_{26}$-$N_{43}$ = -23.918° | $C_{12}$-$C_{11}$-$C_{26}$-$N_{40}$ = -24.794° | $C_{12}$-$C_{11}$-$C_{26}$-$N_{37}$ = -25.612° |
| (-0.002°, 0.001°) | (-0.002°, -0.003°) | (0.428°, 0.464°) |
| $C_{12}$-$C_{11}$-$C_{26}$-$O_{27}$ = 153.089° | $C_{12}$-$C_{11}$-$C_{26}$-$O_{27}$ = -152.123° | $C_{12}$-$C_{11}$-$C_{26}$-$O_{27}$ = 151.101° |
| (179.998°, -179.996°) | (179.999°, 179.995°) | (-179.521°, -179.465°) |
| $N_{44}$-$C_{28}$-$C_{29}$-$C_{31}$ = -2.349° | $N_{41}$-$C_{28}$-$C_{29}$-$C_{31}$ = -1.972° | $N_{38}$-$C_{28}$-$C_{29}$-$C_{31}$ = -2.618° |
| (-0.003°, 0.002°) | (-0.007°, 0.006°) | (0.700°, 0.467°) |
| $O_{27}$-$C_{28}$-$C_{29}$-$C_{30}$ = -2.729° | $O_{27}$-$C_{28}$-$C_{29}$-$C_{30}$ = -2.201° | $O_{27}$-$C_{28}$-$C_{29}$-$C_{30}$ = -3.058° |
| (-0.003°, -0.002°) | (-0.006°, 0.005°) | (0.0290°, 0.180°) |

**Figure 7.** Optimized geometries of molecules **4**–**6** at the B3LYP/6-311g(d,p) level in the gas phase. Hydrogens are omitted for clarity. To compare $S_0$, $S_1$, $T_1$ states, all geometries at the PBE0/6-31+g(d,p) level of theory in chloroform solvent are considered. (Torsion angles in singlet and triplet excited-state optimized geometries are given in parentheses ($S_1$, $T_1$).)

**Table 5. Electrochemical Data of Compounds 4–6**

| compd[a] | $E_{ox}^{onset}$[b] (V) | IP[c] (eV) | $E_{red}^{onset}$[d] (V) | EA[e] (eV) | HOMO[f] (eV) | LUMO[f] (eV) | $\mu_{ground}$[f] (Debye) |
|---|---|---|---|---|---|---|---|
| **4** | 1.32 | 5.72 | −1.52 | 2.88 | −5.67 | 2.30 | 3.96 |
| **5** | 1.3 | 5.7 | −1.5 | 2.9 | −5.67 | 2.29 | 3.99 |
| **6** | 1.4 | 5.8 | −1.48 | 2.92 | −5.69 | 2.31 | 5.48 |

[a]Cyclic voltammetry was performed to calculate IP and EA of **4**–**6** in 0.1 M $NBu_4ClO_4$ in anhydrous DCM solvent. [b]Onset potential of oxidation. [c]IP = $-(E_{ox}^{onset} + 4.4)$ eV. [d]Onset potential of reduction. [e]EA = $-(E_{red}^{onset} + 4.4)$ eV. [f]Calculated at the B3LYP-6-311G(d,p) level of theory in the gas phase.

**Scheme 2. Energy-Level Diagram of the Materials Used in the Devices: (a) Pyrene As Emitter Material; (b) Compound 5 as Emitter and ETL Material; (c) Compound 5 and $Alq_3$ as ETL**

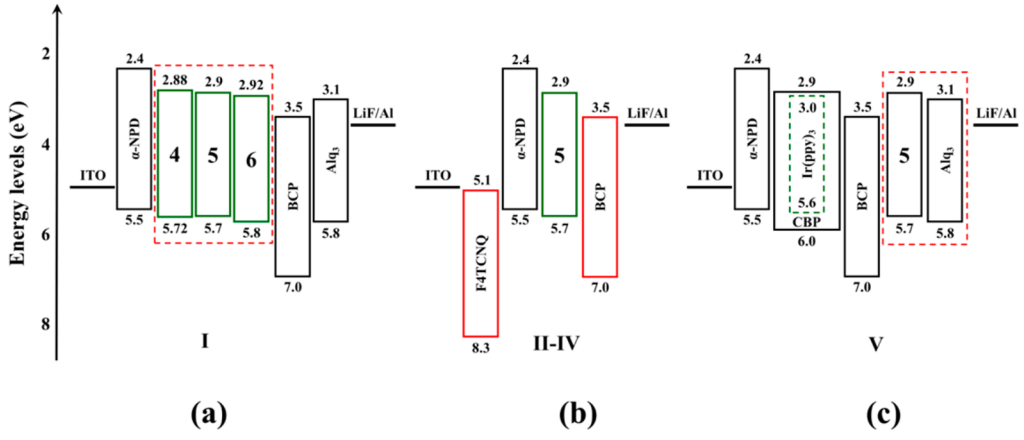


and 478 nm in **6** and are in very good agreement with the experimental emissions.

To assess the possibility of triplet to singlet intersystem crossing, the energy gap between lowest excited singlet state and lowest triplet state ($\Delta E_{ST}$) is calculated. $\Delta E_{ST}$ is 165, 165, and 153 meV for molecules **4**, **5**, and **6** respectively, and it is 173 meV for **7** and 259 meV for unsubstituted pyrene. There is an obvious decrease in the $\Delta E_{ST}$ upon introduction of substituents on basic pyrene and a further decrease upon addition of methoxy substituents on the molecules. In general, the molecules **4**–**6** show proficiently smaller $\Delta E_{ST}$, facilitating $T_1$–$S_1$ reverse intersystem crossing.

**Electrochemical Properties.** Electrochemical properties of the molecules were studied (SI) to estimate the ionization



DOI: 10.1021/acs.joc.5b02423
J. Org. Chem. 2016, 81, 603–614

potential (IP) and the electron affinity for compounds **4**–**6** using cyclic voltammetry (CV) in a standard three-electrode electrochemical cell, and the results are summarized in Table 5. The onset oxidation potentials of **4**–**6** were estimated to be ~1.3 V, corresponding to the IP ~5.7 eV (Table 5). The very small variation in IP value indicates that the oxidation occurs from the same moiety in all the molecules, namely pyrene. The onset reduction potentials were estimated to be ~1.5 V, corresponding to the EA of ~2.9 eV. IP and EA estimated by CV can be correlated to the HOMO and LUMO energy values obtained from DFT calculations. Hence, for comparison of the experimental values, the frontier orbital data obtained from DFT are given in Table 5 as well. While the HOMO values obtained from DFT are in good agreement with the IP obtained from CV measurements, the LUMO values are slightly underestimated by the DFT method. EA using DFT methods are underestimated, and here, this could also be due to the different conformations adopted by the molecule in the solvent (the variation of LUMO with change in geometry is larger in these molecules).[52] Scheme 2 depicts the typical energy level diagram for a bilayer device with 4,4′-bis[*N*-(1-naphthyl)-*N*-phenyl-l-amino]biphenyl (*α*-NPD) as the hole-transport layer (HTL) and synthesized materials as n-type emitters. The IP of compounds offer a minimal energy barrier for holes to be injected from *α*-NPD, while EA is relatively closer to the work function of cathode LiF/Al. The HOMO and LUMO energy levels of the host materials were estimated from their oxidation onset and first reduction onset potentials.

**Thermal Properties.** The thermal properties like decomposition temperature ($T_d$), melting temperature ($T_m$), and glass transition temperatures ($T_g$) of the compounds (**4**–**6**) were evaluated using thermogravimetric analysis (TGA) and differential scanning calorimetry (DSC) measurements (SI). The data generated showed that the $T_d$ values are in the range of 314–363 °C (Table 6) for these materials, indicating their excellent thermal stability over a wide range of temperatures. No glass transition was noticed for **4** and **6**, while compound **5** had a low $T_g$ value.

**Table 6. Thermal Properties of Compounds 4–6**

| compd | $T_g$[a] (°C) | $T_m$[b] (°C) | $T_d$[c] (°C) |
|---|---|---|---|
| **4** | | 182 | 314 |
| **5** | 52 | 178 | 354 |
| **6** | | 194 | 363 |

[a]$T_g$: glass transition temperature (not observed). [b]$T_m$: melting point. [c]$T_d$: decomposition temperature (corresponding to 5% weight loss).

**Electrochemiluminescence.** To study the utility of the synthesized pyrene derivatives in device applications, undoped OLEDs were fabricated and characterized. The related HOMO/LUMO energy levels of the materials are illustrated in Scheme 2. The electrochemiluminescent properties of pyrene derivatives **4**–**6** as green emitters were evaluated by fabricating OLEDs with the device configuration I: indium tinoxide (ITO) (120 nm)/4,4′-bis[*N*-(1-naphthyl)-*N*-phenyl-l-amino]biphenyl (*α*-NPD) (30 nm)/pyrene-oxadiazole (35 nm)/bathocuproine (BCP)(6 nm)/tris(8-hydroxyquinoline)-aluminum ($Alq_3$) (35 nm)/LiF(1 nm)/Al(150 nm). Here, ITO (indium–tin oxide) was used as a transparent anode, *α*-NPD as the hole-transporting layer (HTL), BCP (bathocuproine) as the hole-blocking layer (HBL), and tris(8-hydroxyquinoline) aluminum ($Alq_3$) as the electron-transporting layer (ETL); LiF(lithium fluoride) and Al(aluminum) were used as the electron-injecting layer (EIL) and cathode, respectively. The current density–voltage–luminance (J–V–L) characteristics of the fabricated OLEDs are shown in Figure 8a. The characteristics of the current density as a function of applied voltage reveal good diode behavior. The devices utilizing **4**, **5** and **6** as emitter materials exhibit drive voltages (corresponding to 1 cd/m$^2$) of 3.28, 3.17, and 2.98 V, respectively. The current density–luminance (J–L) characteristics (Figure 8b) show a linear relationship. The current, power, and external quantum efficiencies for all the devices along with other parameters of the devices are summarized in Table 7. Out of the three derivatives investigated, the device fabricated with **5** as emissive material showed the highest luminance ($L_{max}$) of 6627 cd/m$^2$, current efficiency ($\eta_c$) of 13.27 cd/A, power efficiency ($\eta_p$) of 9.73 lm/W, and external quantum efficiency ($\eta_{ext}$) of 4.99%. The ECL spectra of the devices with **4**, **5**, and **6** as emitter materials with green light emission with peaks centered at 522, 518, and 527 nm, respectively, with full-width at half maxima (fwhm) of ~60 nm. The narrow fwhm in ECL spectra suggest that the derivatives are capable of forming good chromaticity devices. The CIE chromaticity coordinates of the derivatives as ECL materials are determined using the ECL spectra of the devices at 10 V. The chromaticity diagram is shown in Figure 9, and the CIE coordinates are tabulated in Table 7. It can also be observed from Figure 7 that the variation of applied voltage has

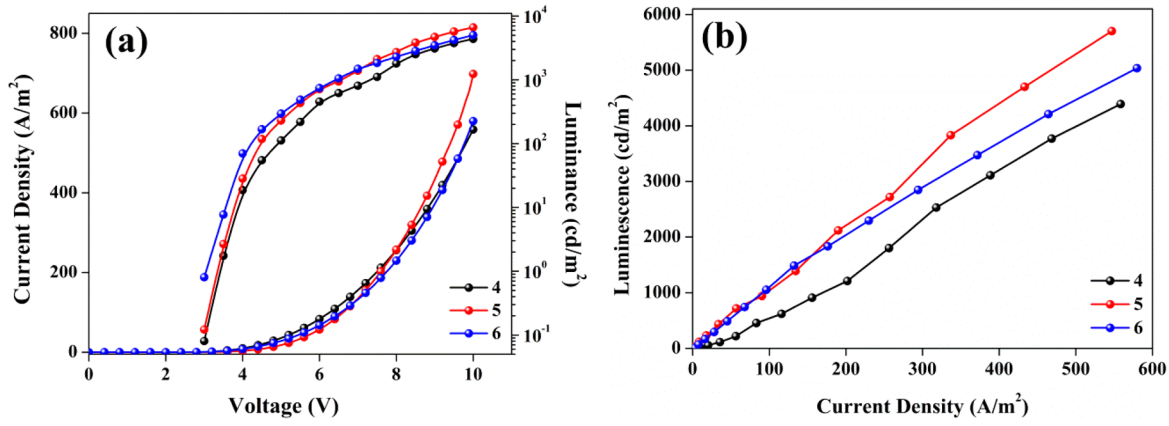


**Figure 8.** (a) Current density–voltage–luminance (J–V–L); (b) Current density–luminance (J–L) characteristics for OLEDs with pyrene as EL material.



DOI: 10.1021/acs.joc.5b02423
*J. Org. Chem.* 2016, 81, 603–614

**Table 7. Electroluminescent Performance Data of Pyrene Derivatives As Emissive Materials**

| device[a] | $V_{onset}$[b] (V) | $L_{max}$[c] (cd m$^{-2}$) | $\eta_c$ (cd A$^{-1}$)[d] | $\eta_p$[e] (lm W$^{-1}$) | $\eta_{ext}$[f] (%) | $\lambda_{em}$[g](fwhm) (nm) | CIE$_{(x,y)}$[h] |
|---|---|---|---|---|---|---|---|
| **4** | 3.28 | 4390 | 10.86 (8 V) | 6.93 (6 V) | 4.25 (8 V) | 522 (58) | (0.311, 0.588) |
| **5** | 3.17 | 6627 | 13.27 (8 V) | 9.73 (5.5 V) | 4.99 (8 V) | 518 (56) | (0.271, 0.547) |
| **6** | 2.98 | 5034 | 11.24 (7 V) | 7.42 (4.5 V) | 3.46 (7 V) | 527 (62) | (0.323, 0.572) |

[a]Device configuration I: ITO (120 nm)/$\alpha$-NPD (30 nm)/**5** (35 nm)/BCP (6 nm)/$Alq_3$ (35 nm)/LiF (1 nm)/Al (150 nm). [b]$V_{onset}$: turn-on voltage at luminance of 1 cd m$^{-2}$. [c]$L_{max:}$ maximum luminance at 10 V. [d]$\eta_c$: maximum current efficiency measured at applied voltage (in parentheses). [e]$\eta_p$: maximum power efficiency measured at applied voltage (in parentheses). [f]$\eta_{ext}$: maximum external quantum efficiency measured at applied voltage (in parentheses). [g]$\lambda_{em}$: emission wavelength maximum. fwhm: full width half-maximum at 10 V. [h]CIE color coordinate.

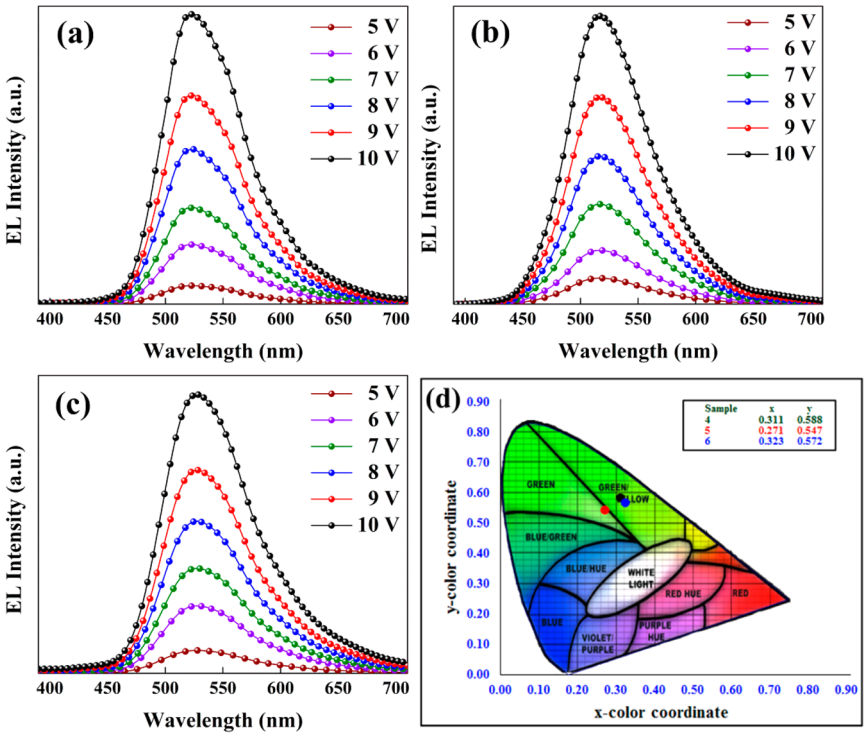


**Figure 9.** EL spectra of the OLEDs with pyrene derivatives (a) **4** (b) **5**, and (c) **6** as EL materials at different applied voltages and (d) chromaticity diagram.

no effect on the shape and the peak of the ECL spectra. Compared to the thin film, fluorescence spectra with the ECL emission peaks for all the derivatives may be ascribed to the intermolecular interactions in the excited states.[53]

The role of pyrene derivatives as electron-transporting and -emitting materials were studied by fabricating OLEDs with the device configurations II–IV: ITO (120 nm)/2,3,5,6-tetrafluoro-7,7,8,8-tetracyanoquinodimethane ($F_4TCNQ$) (4 nm)/$\alpha$-NPD (40 nm)/pyrene (50 nm)/BCP (6 nm)/LiF (1 nm)/Al (150 nm). Here, $F_4TCNQ$ (2,3,5,6-tetrafluoro-7,7,8,8-tetracyanoquinodimethane) acts as a hole-injecting layer (HIL). An optimized thickness of $F_4TCNQ$ was used for better hole injection as reported previously.[54] The device performance data are presented in Table 8. It is evident from Table 8 that device II without $F_4TCNQ$ and BCP has low efficiencies of 2.67 cd A$^{-1}$ ($\eta_c$), 1.36 lm W$^{-1}$ ($\eta_p$), and 0.77% ($\eta_{ext}$). With the inclusion of 4 nm of $F_4TCNQ$ layer (device III) there is an increase of efficiencies: 13.56 cd A$^{-1}$ ($\eta_c$), 9.56 lm W$^{-1}$ ($\eta_p$), and 5.34% ($\eta_{ext}$). This can be ascribed to the efficient injection of holes from the ITO anode to the hole transport layer $\alpha$-NPD.[54−56] Furthermore, in device IV, with the use of BCP as a HBL, there is a further increase in the efficiencies. This increase in efficiencies may be due to the confining of redundant holes in the emitting layer which did not recombine with the electrons in the emitting zone.[57] The device structure IV was used for the other two derivatives (**4** and **6**). It is evident from

**Table 8. Electroluminescent Performance Data of OLEDs Using Pyrene as Both EL and ETL Material**

| device | $V_{onset}$[d] (V) | $L_{max}$[e] (cd m$^{-2}$) | $\eta_c$[f] (cd A$^{-1}$) | $\eta_p$[g] (lm W$^{-1}$) | $\eta_{ext}$[h] (%) |
|---|---|---|---|---|---|
| **5**[a] | 6.78 | 809 | 2.67 (9.0) | 1.36 (8.5) | 0.77 (9.5) |
| **5**[b] | 3.23 | 7605 | 13.56 (7.0) | 9.56 (6.5) | 5.34 (7.0) |
| **5**[c] | 2.76 | 8524 | 15.13 (7.5) | 10.95 (6.5) | 5.96 (7.5) |
| **4**[c] | 2.93 | 6387 | 13.06 (8.5) | 8.34 (5.5) | 5.14 (8.5) |
| **6**[c] | 2.61 | 7050 | 14.30 (7.5) | 9.46 (5.0) | 5.49 (7.5) |

[a]Device configuration II: ITO (120 nm)/$\alpha$-NPD (40 nm)/**5**(50 nm)/LiF (1 nm)/Al (150 nm). [b]Device configuration III: ITO (120 nm)/$F_4TCNQ$ (4 nm)/$\alpha$-NPD (40 nm)/**5** (50 nm)/ LiF (1 nm)/Al (150 nm). [c]Device configuration IV: ITO (120 nm)/$F_4TCNQ$ (4 nm)/$\alpha$-NPD (40 nm)/pyrene (50 nm)/BCP (6 nm)/LiF (1 nm)/Al (150 nm) [d]$V_{onset}$: turn-on voltage at luminance of 1 cd m$^{-2}$. [e]$L_{max:}$ maximum luminance at 10 V. [f]$\eta_c$: maximum current efficiency measured at applied voltage (in parentheses). [g]$\eta_{p:}$: maximum power efficiency measured at applied voltage (in parentheses). [h]$\eta_{ext:}$: maximum external quantum efficiency measured at applied voltage (in parentheses).



DOI: 10.1021/acs.joc.5b02423
J. Org. Chem. 2016, 81, 603−614

**Table 9. Electroluminescent Performance Data of OLEDs Using Triplet Emitter $Ir(ppy)_3$ Doped with CBP (with Changing ETL)**

| device[a] | $V_{onset}$[b] (V) | $L_{max}$[c] (cd $m^{-2}$) | $\eta_c$[d] (cd $A^{-1}$) | $\eta_p$[e] (lm $W^{-1}$) | $\eta_{ext}$[f] (%) | $\lambda_{em}$[g] (nm) |
|---|---|---|---|---|---|---|
| without ETL | 12.76 | 1714 | 5.39 (19 V) | 1.23 (18 V) | 0.94 (18 V) | 516 |
| $Alq_3$ | 9.09 | 9650 | 9.79 (20 V) | 2.71 (19 V) | 1.70 (18 V) | 516 |
| **5** | 8.24 | 12769 | 10.10 (19 V) | 3.04 (18 V) | 1.73 (19 V) | 516 |

[a]Device configuration II: ITO (120 nm)/$\alpha$-NPD (40 nm)/$Ir(ppy)_3$-doped CBP (35 nm)/BCP (6 nm)/without ETL, $Alq_3$, or **5** (30 nm)/LiF (1 nm)/Al (150 nm). [b]$V_{onset}$: turn-on voltage at luminance of 1 cd $m^{-2}$. [c]$L_{max:}$ maximum luminance at 21 V. [d]$\eta_c$: maximum current efficiency measured at applied voltage (in parentheses). [e]$\eta_p$: maximum power efficiency measured at applied voltage (in parentheses). [f]$\eta_{ext}$: maximum external quantum efficiency measured at applied voltage (in parentheses). [g]$\lambda_{em}$: emission wavelength maximum at 21 V.

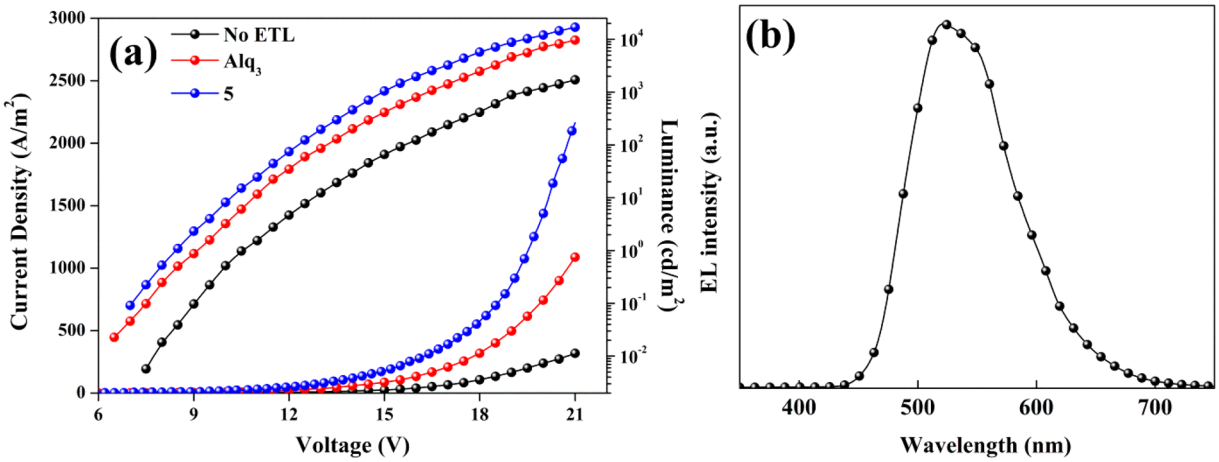


**Figure 10.** (a) Current density−voltage-luminance (J−V-L) characteristics of triplet emitter $Ir(ppy)_3$ doped with CBP without ETL/with $Alq_3$/TBUT as ETL (b) EL spectra of triplet emitter $Ir(ppy)_3$ doped with CBP without ETL/with $Alq_3$/5 as ETL.

Table 8 that the devices show high efficiencies close to 15 cd $A^{-1}$ ($\eta_c$), 11 lm $W^{-1}$ ($\eta_p$), and 6% ($\eta_{ext}$).

The electron-transporting properties of pyrene derivatives were investigated by fabricating three different devices with tris[2-phenylpyridinato-C2,N]iridium(III) ($Ir(ppy)_3$) doped 4,4′-bis(9-carbazolyl)biphenyl (CBP) as phosphorescent emitter with the device configuration V: ITO (120 nm)/$\alpha$-NPD (40 nm)/$Ir(ppy)_3$-doped CBP (35 nm)/BCP (6 nm)/without ETL or **5** or $Alq_3$ (30 nm)/LiF (1 nm)/Al (150 nm). Here, only ETL was changed while the rest of the device configurations were kept the same. The first device was fabricated without any ETL material while the second with $Alq_3$ as ETL and third with **5** as ETL. The data from each of these devices are depicted in Table 9. The J−V−L characteristics and EL spectra of the devices are shown in parts a and b, respectively, of Figure 10. A similar EL spectrum for $Ir(ppy)_3$with $\lambda_{max}$ at 516 nm was observed for all three devices prepared without any ETL, with **5** and $Alq_3$ as electron transporters. It can be seen from Figure 8a and Table 9 that a drastic increase in the luminance and efficiencies can be achieved by the inclusion of ETL in the device configuration. In addition, the device with **5** as ETL shows an increase in luminescence at all voltages and better efficiencies in comparison to $Alq_3$ as ETL. Hence, we can infer that the performance of the device with **5** as ETL is superior compared to commercially available $Alq_3$.

## CONCLUSION

Three new pyrene−oxadiazole compounds **4**−**6** were synthesized and characterized, and their optical, thermal, and electrochemical properties were evaluated. The excellent emissive nature of the compounds studied coupled with their good thermal and electrochemical properties make them suitable candidates for OLEDs as electron-transporting and green-emitting materials. The device performance is improved in terms of current efficiency 13.56 cd $A^{-1}$ ($\eta_c$), power efficiency 9.56 lm $W^{-1}$ ($\eta_p$), and quantum yield 5.34% ($\eta_{ext}$) by using $F_4TCNQ$ as hole-injecting and BCP as hole-blocking agents. The triplet states could be harnessed, which was evident by the delayed fluorescence emission at room temperature. The excellent overlap between the phosphorescence of 2-*p*-tolyl-1,3,4-oxadiazole (**7**) and fluorescence of pyrene leads to reverse intersystem crossing. The excited-state charge-transfer nature of the compound can facilitate the triplet to singlet energy transfer and result in red shifting the emission to green region. The green emission as observed in the film state can also arise due to formation of pyrene excimers.

## EXPERIMENTAL SECTION

**Synthesis and Characterization.** All chemicals are reagent/analytical grade and used without further purification. $^1H$ and $^{13}C$ NMR were recorded on a 75 MHz spectrometer in $CDCl_3$ with TMS as the internal standard. Mass spectra was obtained using electron ionization (EI) ion-trap mass spectrometry.

*Synthesis of 1-Bromopyrene (1).*[42] To a stirred solution of pyrene (10.0 g, 49.5 mmol) in methanol and diethyl ether mixture (60 mL, 1:1), hydrobromic acid (9.2 mL of 48% aqueous solution, 54.4 mmol), and hydrogen peroxide (5.6 mL of 30% aqueous solution, 49.5 mmol) was added over a period of 15 min at 5−10 °C temperature. After complete addition, the reaction mixture was allowed to reach room temperature and stirred at room temperature for 12 h. The reaction progress was monitored by TLC. After the maximum conversion to monobromopyrene, water (50 mL) was added to the reaction mixture, and the compound was extracted with DCM (3 × 100 mL). The combined organic layers were dried over anhydrous $Na_2SO_4$ and filtered, and the solvent was removed under reduced pressure. Thus, the obtained residue was subjected to column chromatography (60−


DOI: 10.1021/acs.joc.5b02423
J. Org. Chem. 2016, 81, 603−614

120 mesh size silica) using hexane as eluent to obtain pure compound. Yield: 86% (11.9 g, colorless solid). Mp: 81−83 °C. $^1$H NMR (300 MHz, $CDCl_3$): $\delta$ 8.43 (d, $J$ = 9.8 Hz, 1H), 8.25−8.13 (m, 4H), 8.11−7.98 (m, 4H).

*Synthesis of Pyrene-1-carbonitrile (**2**).*[43] A mixture of CuCN (3.16 g, 35.37 mmol) and 1-bromopyrene (5 g, 17.685 mmol) in 30 mL of dry DMF was charged into a single-neck RB flask. The reaction mixture was refluxed for 24 h. The reaction mass was then cooled to room temperature, and 30% aq $NH_3$ solution (60 mL) was added. The precipitate obtained was filtered and washed with dilute aq ammonia solution (10 mL) and then with water. This precipitate was then washed with dichloromethane thoroughly. The dichloromethane filtrate was dried over sodium sulfate, and the solvent was removed by rotary evaporator. The residue obtained was purified by column chromatography on silica gel 60−120 mesh, initially using 2% $CHCl_3$/hexane and cautiously increasing the polarity to 10% $CHCl_3$/hexane. The compound obtained had a dark brown tinge which was removed by washing the solid with hexane. The compound was recrystallized twice from toluene to give fluorescent green crystals. Yield: 1.93 g, 48%. $^1$H NMR (300 MHz, $CDCl_3$, ppm): $\delta$ 8.48 (d, 1H), 8.37−8.23 (m, 5H), 8.21−8.10 (m, 3H). MS (ES+): $m/z$ 226 ($M^+$).

*Synthesis of 5-(Pyren-1-yl)-1H-tetrazole (**3**).*[44] A mixture of pyrene-1-carbonitrile (1g, 4.42 mmol), $NaN_3$, (0.43g, 6.63 mmol), and $Bu_3SnCl$ (1.79 mL, 6.63 mmol) in $m$-xylene (30 mL) was refluxed for 24 h under nitrogen atmosphere. The reaction mixture was cooled to room temperature and acidified with 40 mL of 2 N HCl. A white solid suspension was formed, filtered on a Buchner funnel, and washed thoroughly with water followed by $n$-hexane to obtain the title compound as a colorless solid. Yield: 0.82 g, 96%. Mp: 162 °C. $^1$H NMR (300 MHz, $CDCl_3$, ppm): $\delta$ 8.43 (d, $J$ = 9.8 Hz, 1H), 8.25−8.13 (m, 4H), 8.11−7.98 (m, 4H), 7.71. $^{13}$C NMR (75 MHz, $CDCl_3$, ppm): $\delta$ 163.5, 134.32, 133.3, 128.8, 126.6, 126.3, 125.6, 124.8, 123.3, 121, 120.4. MS (ES+): $m/z$ 271 $(M + H)^+$.

**General Procedure A: Compounds Obtained from Tetrazole Derivatives 4−6.** To a stirred solution of pyrenyl-1*H*-tetrazole derivative **3** (1 equiv) in dry pyridine were added benzoyl chloride (1.2 equiv) derivatives slowly via syringe under nitrogen atmosphere. The reaction temperature was raised to reflux and continued for 6 h. Later, it was slowly brought to ambient temperature, and then 20 mL of water was added to the reaction mixture to precipitate out the white solid compound. The reaction mass was filtered, washed thoroughly with water, dried, and purified by silica gel column chromatography using ethyl acetate/hexane (1:10) as eluent. The obtained solid was further recrystallized from toluene/$n$-hexane to obtain the titled compounds as colorless solids.

*Synthesis of 2-(Pyren-1-yl)-5-p-tolyl-1,3,4-oxadiazole (**4**).* Compound **4** was synthesized according to procedure A. Yield: 0.97g, 73%. Mp: 180−182 °C. $^1$H NMR (300 MHz, $CDCl_3$, ppm): $\delta$ 9.6 (d, $J$ = 9.3 Hz, 1H), 8.70 (d, $J$ = 8.0 Hz, 1H), 8.33−8.26 (m, 4H), 8.20 (d, $J$ = 9.0 Hz, 1H), 8.15−8.07 (m, 4H), 7.39 (d, $J$ = 7.7 Hz, 2H), 2.48 (s, 3H). $^{13}$C NMR (75 MHz, $CDCl_3$, ppm): $\delta$ 165.0, 164.4, 142.3, 129.8, 129.5, 129.4, 127.1, 127.0, 126.5, 126.3, 125.2,124.6, 116.9, 21.7. MS (ESI) calcd for $m/z$ 360 [$M^+$]. EI-HRMS: $m/z$ calcd for $C_{25}H_{16}N_2O$ 360.12626 $[M]^+$, found 360.12615 (SI).

*Synthesis of 2-(4-tert-Butylphenyl)-5-(pyren-1-yl)-1,3,4-oxadiazole (**5**).* Compound **5** was synthesized according to procedure A. Yield: 1.13 g, 76%. Mp: 178−181 °C. $^1$H NMR (300 MHz, $CDCl_3$, ppm): $\delta$ 9.58 (d, $J$ = 9.3 Hz, 1H), 8.69 (d, $J$ = 8.1 Hz, 1H), 8.30 (t, $J$ = 7.7 Hz, 2H), 8.27 (d, $J$ = 8.2 Hz, 2H), 8.20−8.17 (m, 3H), 8.12−8.06 (m, 2H), 7.61 (d, $J$ = 8.5 Hz, 2H), 1.41 (s, 9H). $^{13}$C NMR (75 MHz, $CDCl_3$, ppm): $\delta$165.0, 164.3, 155.3, 133.5, 131.1, 129.7, 129.4, 126.3, 126.2, 126.0, 125.1, 124.6, 124.1, 121.1, 116.9, 35.1, 31.1. MS (ESI) calcd for $m/z$ 402 [$M^+$]. EI-HRMS: $m/z$ calcd for $C_{28}H_{22}N_2O$ 402.17321 $[M]^+$, found 402.17315 (SI)

*Synthesis of 2-(Pyren-1-yl)-5-(3,4,5-trimethoxyphenyl)-1,3,4-oxadiazole (**6**).* Compound **6** was synthesized according to procedure A. Yield: 1.1 g, 69%. Mp: 203−205 °C. $^1$H NMR (300 MHz, $CDCl_3$, ppm): $\delta$ 9.57 (d, $J$ = 9.8 Hz, 1H), 8.69 (d, $J$ = 8.3 Hz, 1H). 8.36−8.28 (m, 4H), 8.22 (d, $J$ = 8.2 Hz 1H), 8.15−8.07 (m, 2H), 7.48 (s, 1H), 4.03 (s, 6H), 3.97 (s, 3H). $^{13}$C NMR (75 MHz, $CDCl_3$, ppm): $\delta$ 165.0, 164.3, 142.3, 131.1, 127.1, 127.0, 126.4, 126.3, 126.2, 125.1, 124.9, 124.6, 130.5, 129.8, 129.5, 129.39, 124.1, 116.9, 21.7. MS (ESI) calcd for $m/z$ 436[$M^+$]. EI-HRMS: $m/z$ calcd for $C_{27}H_{20}N_2O_4$, 436.14231 $[M]^+$, found 436.14220 (SI)

*Synthesis of 2-p-Tolyl-1,3,4-oxadiazole (**7**).*[58−60] To a solution of the $p$-toluenebenzoic acid (0.01 mol) in anhydrous methanol (25 mL) was added sulfuric acid (0.015 mol), and the mixture was refluxed for 6 h. The solvent was evaporated, and the ester formed was used in the next step without purification. To the crude ester was added hydrazine hydrate (0.025 mol), and this mixture was kept at room temperature until a precipitate of acyl hydrazide was formed. The solid was filtered off and dried in vacuum. The hydrazide was heated in trimethyl orthoformate (30 mL) for 10 h under reflux, the solvent was evaporated, and the oily residue was distilled in vacuum. The product that solidified in the condenser was recrystallized from acetone and hexane to obtain 2-$p$-tolyl-1,3,4-oxadiazole.[58−60] Yield: 1.2 g, 88%, mp 87 °C. $^1$H NMR (300 MHz, $CDCl_3$, ppm): $\delta$ 8.45 (s, 1H), 7.97 (d, 2H), 7.33 (d, 2H), 2.43 (s, 3H). $^{13}$C NMR (75 MHz, $CDCl_3$, ppm): $\delta$ 164.9, 152.4, 142,6, 120.7, 129.81, 127.0, 21.7.

**Thermal and Electrochemical analysis.** The glass transition temperature ($T_g$) of the compounds was measured using differential scanning calorimetry (DSC) under a nitrogen atmosphere and at a heating rate of 10 °C min$^{-1}$. The $T_g$ was determined from the second heating scan. Thermogravimetric analysis (TGA) was performed using in the temperature range of 30−550 °C under a nitrogen atmosphere at a heating rate of 10 °C min$^{-1}$. Cyclic voltammetric measurements were performed on a PC-controlled electrochemical analyzer. Cyclic voltammetric experiments were performed in 1 mM solution of degassed dry dichloromethane at a scan rate of 100 mV s$^{-1}$ using 0.1 M tetrabutylammonium perchlorate (TBAP) as the supporting electrolyte. The glassy carbon was used as the working electrode, Ag/AgCl as the reference electrode, and platinum wire as the counter electrode. The working electrode surface was first polished with 1 mm alumina slurry, followed by 0.3 mm alumina slurry on a microcloth. It was then rinsed with Millipore water and also sonicated in water for 5 min. The polishing and sonication steps were repeated twice. CV data for all the samples was calibrated using ferrocene as standard.

**Spectroscopic Methods.** UV−vis absorption and fluorescence measurements were carried out in different solvents at room temperature. Thin films were prepared by spin coating $10^{-2}$ M solution of the samples in chloroform at 1000 rpm for 1 min. Spectra were measured using a UV−vis spectrophotometer. Steady-state fluorescence, phosphorescence, and triplet lifetimes were recorded using spectrofluorometer. Phosphorescence measurements were carried out in a glassy solvent 1:1 ethanol/methanol using 0.06 ms delay, 61 ms time per flash, and flash count 100. The fluorescence quantum yields of **4**, **5**, and **6** in cyclohexane were determined using 9,10-diphenylanthracene ($\Phi_r$ = 0.95, in cyclohexane)[61] as a standard by exciting at 390 nm, and the values were obtained using the following equation

$$\Phi_f = \Phi_r \frac{I_s}{I_r}\frac{A_r}{A_s}\frac{\eta_r^2}{\eta_s^2} \qquad \text{(eq 1)}$$

where $\Phi_f$ is the fluorescence quantum yield of the sample, $A$ is the absorbance of the solution, $I$ is the integral area of the emission peak, $\eta$ is the refractive index of the solution, and the subscripts of "s" and "r" refer to the solutions of the sample and reference, respectively. Time-correlated single-photon counting was used to measure the fluorescence lifetime in the nanosecond time scale. The femtosecond pulses at 8 MHz repetition rate were obtained from fractional part of MaiTai output passing through femtosecond pulse selector. The excitation pulses at 370 nm were generated by frequency doubling the 740 nm Ti-sapphire output with 0.5 mm BBO crystal. These excitation pulses are focused to the sample using a Fluorescence Up-conversion set up. The time distribution data of fluorescence intensity were recorded on a SPC-130 TCSPC module. The instrument response function was 250 fs.

**Computational Methods.** All calculations are performed using Gaussian09[62] software. The ground-state neutral geometries were


DOI: 10.1021/acs.joc.5b02423
J. Org. Chem. 2016, 81, 603−614

optimized at the B3LYP[63−65]/6-311g(d,p) level of theory. Vibrational frequencies were computed and resulted in no imaginary frequencies; thus, these ground-state-optimized geometries correspond to minima on the potential energy surface. At this geometry, singlet excitation energies were calculated using TDDFT, at the PBE0[66]/6-311g(d,p) level of theory, in $CHCl_3$ solvent by means of the default linear response PCM model (LR-PCM).[67,68] Emission energies are calculated at state-specific PCM (SS-PCM) level, using PBE0 functional, with a 6-31+g(d,p) basis set. The diffuse function (+) here is used for the better description of excited states. Along with this, an ultrafine grid is used for numerical integrations. The percentage contributions of pyrene and nonpyrene moieties to the respective molecular orbitals are calculated using GaussSum.[69]

**Device Fabrication.** The electroluminescent properties of the pyrene derivatives were studied by fabricating undoped OLEDs using thermal evaporation at a base pressure of $5 \times 10^{-6}$ Torr. Patterned ITO coated glass substrates with a sheet resistance of 15 Ω/□ were used as anodes, which were cleaned and UV−Ozone treated as reported earlier.[56] On the ITO substrate, the HIL, HTL, emitting layer, HBL, ETL, EIL, and cathode were deposited sequentially without breaking the vacuum. $F_4TCNQ$ was used as HIL, α-NPD was used as the HTL, BCP was used as HBL, $Alq_3$ was used as ETL, LiF was used as EIL, and Al was used as the cathode. The deposition rate of organic materials was maintained at 0.5 Å $s^{-1}$, whereas the deposition rates of LiF and Al were 0.1 Å $s^{-1}$ and 6 Å $s^{-1}$ respectively. The deposition rate and thickness of the deposited layers were controlled *in situ* by a quartz crystal thickness monitor. The cathode was deposited on the top of the structure through a shadow mask. The active area of the device was 1.6 $mm^2$. The EL spectra, J−V−L characteristics of the devices were measured using a spectrophotometer, a computer controlled, programmable source meter and Si photodiode. All of the measurements were carried out at room temperature under ambient conditions without any encapsulation.

## ■ ASSOCIATED CONTENT

### Supporting Information

The Supporting Information is available free of charge on the ACS Publications website at DOI: 10.1021/acs.joc.5b02423.

$^1H$, $^{13}C$ NMR, and HRMS spectra of the newly synthesized compounds, optical spectra of the compounds recorded in different solvents, delayed fluorescence lifetimes, thermal and electrochemical data, and isodensity surface plots of frontier molecular orbitals (PDF)

## ■ AUTHOR INFORMATION


### Corresponding Authors

*E-mail: mn.satyanarayan@gmail.com.
*E-mail: bhanu2505@yahoo.co.in.
*E-mail: jrao@iict.res.in.


### Notes

The authors declare no competing financial interest.

## ■ ACKNOWLEDGMENTS

V.J.R., S.C., and A.V. thank CSIR for TAPSUN-NWP0055 project funding. We thank the Director, CSIR-IICT, for encouragement. M.E.M. thanks CSIR-SRA for fellowship. H.U. and M.R.K. acknowledge the Department of Physics, NITK, Surathkal, for various facilities and financial support.

## ■ REFERENCES


(1) Tang, C. W.; VanSlyke, S. A. *Appl. Phys. Lett.* **1987**, *51*, 913.
(2) Burroughes, J. H.; Bradley, D. D. C.; Brown, A. R.; Marks, R. N.; MacKay, K.; Friend, R. H.; Burns, P. L.; Holmes, A. B. *Nature* **1990**, *347*, 539.
(3) Forrest, S. R.; Baldo, M. A.; O'Brien, D. F.; You, Y.; Shoustikov, A.; Sibley, S.; Thompson, M. E. *Nature* **1998**, *395*, 151.
(4) Zhu, M.; Yang, C. *Chem. Soc. Rev.* **2013**, *42*, 4963.
(5) Shih, P. I.; Tseng, Y. H.; Wu, F. I.; Dixit, A. K.; Shu, C. F. *Adv. Funct. Mater.* **2006**, *16*, 1582.
(6) Okumoto, K.; Kanno, H.; Hamaa, Y.; Takahashi, H.; Shibata, K. *Appl. Phys. Lett.* **2006**, *89*, 063504.
(7) Li, Y.; Fung, M. K.; Xie, Z.; Lee, S. T.; Hung, L. S.; Shi, J. *Adv. Mater.* **2002**, *14*, 1317.
(8) D'Andrade, B. W.; Forrest, S. R. *Adv. Mater.* **2004**, *16*, 1585.
(9) Baldo, M. A.; Brien, D. F. O.; You, Y.; Shoustikov, A.; Sibley, S.; Thompson, M. E.; Forrest, S. R. *Nature* **1998**, *395*, 151.
(10) Adachi, C.; Baldo, M. A.; Thompson, M. E.; Forrest, S. R. *J. Appl. Phys.* **2001**, *90*, 5048.
(11) Baldo, M. A.; Adachi, C.; Forrest, S. R. *Phys. Rev. B: Condens. Matter Mater. Phys.* **2000**, *62*, 10967.
(12) Endo, A.; Ogasawara, M.; Takahashi, A.; Yokoyama, D.; Kato, Y.; Adachi, C. *Adv. Mater.* **2009**, *21*, 4802.
(13) Dias, F. B.; Bourdakos, K. N.; Jankus, V.; Moss, K. C.; Kamtekar, K. T.; Bhalla, V.; Santos, J.; Bryce, M. R.; Monkman, A. P. *Adv. Mater.* **2013**, *25*, 3707.
(14) Zhang, Q.; Li, B.; Huang, S.; Nomura, H.; Tanaka, H.; Adachi, C. *Nat. Photonics* **2014**, *8*, 326.
(15) Zhang, Q.; Li, J.; Shizu, K.; Huang, S.; Hirata, S.; Miyazaki, H.; Adachi, C. *J. Am. Chem. Soc.* **2012**, *134*, 14706.
(16) Uoyama, H.; Goushi, K.; Shizu, K.; Nomura, H.; Adachi, C. *Nature* **2012**, *492*, 234.
(17) Sun, Y.; Duan, L.; Zhang, D.; Qiao, J.; Dong, G.; Wang, L.; Qiu, Y. *Adv. Funct. Mater.* **2011**, *21*, 1881.
(18) Gong, S.; Chen, Y.; Zhang, X.; Cai, P.; Zhong, C.; Ma, D.; Qin, J.; Yang, C. *J. Mater. Chem.* **2011**, *21*, 11197.
(19) Tao, Y.; Yang, C.; Qin, J. *Chem. Soc. Rev.* **2011**, *40*, 2943.
(20) Priyanka, B.; Anusha, V.; Bhanuprakash, K. *J. Phys. Chem. C* **2015**, *119*, 12251.
(21) Chen, H. F.; Yang, S. J.; Tsai, Z. H.; Hung, W. Y.; Wang, T. C.; Wong, K. T. *J. Mater. Chem.* **2009**, *19*, 8112.
(22) Kathirgamanathan, P.; Surendrakumar, S.; Vanga, R. R.; Ravichandran, S.; Juan, A.-L.; Ganeshamurugan, S.; Kumaraverl, M.; Paramaswara, G.; Arkley, V. *Org. Electron.* **2011**, *12*, 666.
(23) White, W.; Hudson, Z. M.; Feng, X.; Han, S.; Liu, Z.-H.; Wang, S. *Dalton Trans.* **2010**, *39*, 892.
(24) Tonzola, C. J.; Kulkarni, A. P.; Gifford, A. P.; Kaminsky, W.; Jenekhe, S. A. *Adv. Funct. Mater.* **2007**, *17*, 863.
(25) Mallesham, G.; Swetha, Ch.; Niveditha, S.; Mohanty, M. E.; Jagadeesh Babu, N.; Kumar, A.; Bhanuprakash, K.; Rao, V. J. *J. Mater. Chem. C* **2015**, *3*, 1208.
(26) Chen, C. T.; Wei, Y.; Lin, J. S.; Moturu, M. V. R. K.; Chao, W. S.; Tao, Y. T.; Chien, C. H. *J. Am. Chem. Soc.* **2006**, *128*, 10992.
(27) Ichikawa, M.; Kawaguchi, T.; Kobayashi, K.; Miki, T.; Furukawa, K.; Koyama, T.; Taniguchi, Y. *J. Mater. Chem.* **2006**, *16*, 221.
(28) Thomas, K. R. J.; Kapoor, N.; Bolisetty, M. N. K.; Jou, J.-H.; Chen, Y. L.; Jou, Y. C. *J. Org. Chem.* **2012**, *77*, 3921.
(29) Zhan, Y.; Peng, J.; Ye, K.; Xue, P.; Lu, R. *Org. Biomol. Chem.* **2013**, *11*, 6814.
(30) Figueira-Duarte, T. M.; Mullen, K. *Chem. Rev.* **2011**, *111*, 7260.
(31) Kim, Y. H.; Yoon, D. K.; Lee, E. H.; Ko, Y. K.; Jung, H. T. *J. Phys. Chem. B* **2006**, *110*, 20836.
(32) Wu, K. C.; Ku, P. J.; Lin, C. S.; Shih, H. T.; Wu, F. I.; Huang, M. J.; Lin, J. J.; Chen, I. C.; Cheng, C. H. *Adv. Funct. Mater.* **2008**, *18*, 67.
(33) Thomas, K. R.; Lin, J. T.; Tao, Y. T.; Ko, C. W. *Adv. Mater.* **2000**, *12*, 1949.
(34) Bernhardt, S.; Kastler, M.; Enkelmann, V.; Baumgarten, M.; Mullen, K. *Chem. - Eur. J.* **2006**, *12*, 6117.
(35) Zhao, Z. J.; Li, J. H.; Chen, X. P.; Lu, P.; Yang, Y. *Org. Lett.* **2008**, *10*, 3041.
(36) Lo, M. Y.; Zhen, C.; Lauters, M.; Jabbour, G. E.; Sellinger, A. *J. Am. Chem. Soc.* **2007**, *129*, 5808.




DOI: 10.1021/acs.joc.5b02423
*J. Org. Chem.* 2016, 81, 603−614

(37) Keawin, T.; Prachumrak, N.; Namuangruk, S.; Pansay, S.; Kungwan, N.; Maensiri, S.; Jungsuttiwong, S.; Sudyoadsuk, T.; Promarak, V. *RSC Adv.* **2015**, *5*, 73481.
(38) Chou, P. Y.; Chou, H. H.; Chen, Y. H.; Su, T. H.; Liao, C. Y.; Lin, H. W.; Lin, W. C.; Yen, H. Y.; Chena, I. C.; Cheng, C. H. *Chem. Commun.* **2014**, *50*, 6869.
(39) Salunke, J. K.; Sonar, P.; Wong, F. L.; Roy, V. A. L.; Leec, C. S.; Wadgaonkar, P. P. *Phys. Chem. Chem. Phys.* **2014**, *16*, 23320.
(40) Lo, M. Y.; Zhen, C.; Lauters, M.; Jabbour, G. E.; Sellinger, A. *J. Am. Chem. Soc.* **2007**, *129*, 5808.
(41) Zhan, Y.; Peng, J.; Ye, K.; Xue, P.; Lu, R. *Org. Biomol. Chem.* **2013**, *11*, 6814.
(42) He, C.; He, Q.; Chen, Q.; Shi, L.; Cao, H.; Cheng, J.; Deng, C.; Lin, T. *Tetrahedron Lett.* **2010**, *51*, 1317.
(43) Tsuie, B.; Reddinger, J. L.; Sotzing, G. A.; Soloducho, J.; Katritzky, A. R.; Reynolds, J. R. *J. Mater. Chem.* **1999**, *9*, 2189.
(44) Kricheldorf, H. R.; Leppert, E. *Synthesis* **1976**, *1976*, 329.
(45) Lambert, C.; Ehbets, J.; Rausch, D.; Steeger, M. *J. Org. Chem.* **2012**, *77*, 6147.
(46) Crawford, A. G.; Dwyer, A. D.; Liu, Z.; Steffen, A.; Beeby, A.; Palsson, L.; Tozer, D. J.; Marder, T. B. *J. Am. Chem. Soc.* **2011**, *133*, 13349.
(47) Pati, A. K.; Gharpure, S. J.; Mishra, A. K. *Faraday Discuss.* **2015**, *177*, 213.
(48) Hu, J. Y.; Yamato, T. Synthesis and Photophysical Properties of Pyrene-Based Multiply Conjugated Shaped Light-Emitting Architectures: Toward Efficient Organic-Light-Emitting Diodes. In *Organic Light Emitting Diode - Material, Process and Devices*; Ko, S. H., Ed.; , InTech Publisher, 2011;Chapter 2, CC BY-NC-SA 3.0 license. ISBN: 978-953-307-273-9. DOI: 10.5772/776.
(49) Chen, X. L.; Yu, R.; Zhang, Q.; Zhou, L.; Wu, X.; Zhang, Q.; Lu, C. *Chem. Mater.* **2013**, *25*, 3910.
(50) Zhao, J.; Ji, S.; Guo, H. *RSC Adv.* **2011**, *1*, 937.
(51) Pérez-Prieto, J.; Perez, L. P.; Bejar, M. G.; Mirandab, M. A.; Stiriba, S. *Chem. Commun.* **2005**, 5569.
(52) Zhang, G.; Musgrave, C. B. *J. Phys. Chem. A* **2007**, *111* (8), 1554.
(53) Zhuang, S.; Shangguan, R.; Huang, H.; Tu, G.; Wang, L.; Zhu, X. *Dyes Pigm.* **2014**, *101*, 93.
(54) Fernandes, J. M.; Kiran, M. R.; Ulla, H.; Satyanarayan, M. N.; Umesh, G. *Superlattices Microstruct.* **2014**, *76*, 385.
(55) Fernandes, J. M.; Kiran, M. R.; Ulla, H.; Satyanarayan, M. N.; Umesh, G. *Superlattices Microstruct.* **2015**, *83*, 766.
(56) Ulla, H.; Kiran, M. R.; Garudachari, B.; Satyanarayan, M. N.; Umesh, G.; Isloor, A. M. *Opt. Mater.* **2014**, *37*, 311.
(57) Tomova, R.; Petrova, P.; Topalova, R. S. *Phys. Status Solidi C* **2010**, *3*−*4*, 992.
(58) Nowak-Wydra, B.; Gierczyk, B.; Schroeder, G. *Magn. Reson. Chem.* **2003**, *41*, 689.
(59) Gierczyk, B.; Nowak-Wydra, B.; Grajewski, J.; Zalas, M. *Magn. Reson. Chem.* **2007**, *45*, 123.
(60) Grekov, A. P.; Shvayka, O. P.; Egunova, L. M. *Zh. Obshch. Khim.* **1959**, *29*, 2027.
(61) Morris, J. V.; Mahaney, M. A.; Huber, J. R. *J. Phys. Chem.* **1976**, *80*, 969.
(62) Frisch, M. J.; Trucks, G. W.; Schlegel, H. B.; Scuseria, G. E.; Robb, M. A.; Cheeseman, J. R.; Scalmani, G.; Barone, V.; Mennucci, B.; Petersson, G. A. *Gaussian 09, Revision B.01*; Gaussian, Inc.: Wallingford, CT, 2010.
(63) Becke, A. D. *J. Chem. Phys.* **1993**, *98*, 5648.
(64) Becke, A. D. *J. Chem. Phys.* **1996**, *104*, 1040.
(65) Lee, C. T.; Yang, W. T.; Parr, R. G. *Phys. Rev. B: Condens. Matter Mater. Phys.* **1988**, *37*, 785.
(66) Adamo, C.; Barone, V. *J. Chem. Phys.* **1999**, *110*, 6158.
(67) Miertus, S.; Scrocco, E.; Tomasi, J. *Chem. Phys.* **1981**, *55*, 117.
(68) Cossi, M.; Barone, V.; Cammi, R.; Tomasi, J. *Chem. Phys. Lett.* **1996**, *255*, 327.
(69) O'boyle, N. M.; Tenderholt, A. L.; Langner, K. M. *J. Comput. Chem.* **2008**, *29*, 839.



DOI: 10.1021/acs.joc.5b02423
*J. Org. Chem.* 2016, 81, 603−614